COLLISION AND EVAPORATION AVOIDANCE FOR SPACECRAFT FORMATION

Gianmarco Radice
Department of Aerospace Engineering
University of Glasgow
Glasgow, G12 8QQ
UK

Malcolm Macdonald
Department of Mechanical Engineering
University of Strathclyde
Glasgow, G1 1XJ
UK

ABSTRACT

Formation flying is an extremely promising approach to space operations with the potential to enable new types of missions and providing substantial increase in the performance of future space science and Earth observation applications. To successfully validate formation flying however requires the development of specific technologies and methodologies, which are beyond current state-of-the art in a wide range of diverse fields such as metrology and spacecraft guidance, navigation and control. A number of missions are currently under different stages of development to implement some of these stringent requirements.

The paper develops and compares collision avoidance algorithms, demonstrating them within a 6 degrees of freedom, multi-spacecraft environment. At first a number of different collision avoidance scenarios will be identified alongside the triggers that will cause the algorithms to be activated. Once activated the collision avoidance algorithm must ensure corrective action to avoid catastrophic consequences to the mission.

INTRODUCTION

Formation flying of satellites is an emerging technology for next generation space systems. The cost of launching a satellite depends on the size of the satellite. It becomes prohibitively expensive to launch large satellites. Formation flying technology aims at creating a 'virtual satellite' by a network of small satellites. The virtual satellite thus created, is expected to perform the functions of a large satellite at a much lower cost. Another advantage of formation flying is achieving multi mission capabilities, through the reconfiguration of the formation. Formation flying utilizes many satellites moving in a coordinated fashion to complete missions such as optical interferometry and Earth/Solar observation. In recent years, the concept of using a group of spacecraft flying in a close, precise formation has been considered in numerous future satellite missions. Xeus, Simbol-X, Darwin, Smart-3, Lisa/Lisa-PF, Ace+, Swarm and Apies are some of the proposed formation flying missions.

We will use the Proba-3 mission, as our test case. This is the third in ESA's series of missions for validating developments in space systems while carrying an 'added value' user payload which can directly benefit from the engineering innovations being assessed. Proba-3 will aim to demonstrate the technologies required for formation flying of multiple spacecraft. The mission comprises two independent, a coronograph and an occulter, shown in Figure 1.

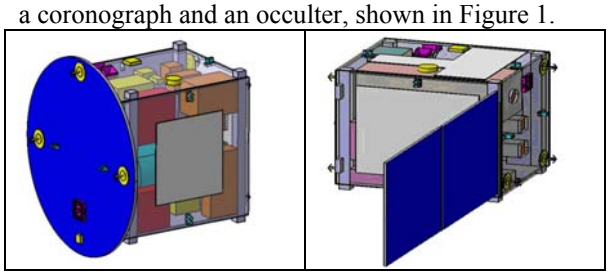

Figure 1. Proba occulter and coronograph.

Utilising either cold gas or electrical thrusters for agile manoeuvring, and both radio frequency (RF) and optical (laser-based) metrology techniques for accurate position measurement and control, the combined system is expected to achieve a relative positioning accuracy of the order of 100 microns over a separation range of 25 to 250 metres. The Proba-3 mission will provide an opportunity to validate the metrology and actuation techniques and technologies and to develop and dynamically verify the guidance strategies and navigation and control algorithms necessary for formation flying during future science, astronomy and Earth observation missions. It will also test a wide range of command and control strategies and provide development and verification tools and facilities. The spacecraft pair will fly a Highly Elliptical Orbit (HEO) divided between periods of accurate formation flying, when payload observations will be possible, and periods of free flight. The relative positions of the two craft will be determined through radio metrology, which functions for separations between 5 metres and 8 kilometres, with an accuracy of a few centimetres. Increased accuracy for separations up to 500 metres will be obtained using optical laser techniques, having both coarse and fine sensors to refine the relative position measurements to an accuracy of hundreds of microns.

PROBA-3 MISSION

The objective of the mission is to demonstrate FF technology while at the same time provide a relevant scientific return. A Highly Elliptical Orbit (HEO) with a period of 24 hours has been selected; its parameters are shown in Table 1.

Parameter	Value
Semi-major axis, *a* (km)	42378.144
Eccentricity, *e*	0.830617
Inclination, *i* (°)	17.8
Right ascension, Ω (°)	68.0
Argument of perigee, ω (°)	180.0

Table 1: Proba-3 parameters

The choice of a HEO was due to its quiet gravitational environment around the apogee, while the 24 hours orbital period was chosen for launch and operational reasons was chosen. The selected HEO can provide e low launch cost, GPS availability around perigee (for initial formation acquisition and back-up during the experimental mission phases), acceptable in-orbit disturbance level, quiet environment for accurate FF demonstrations and experiments at the apogee region, and minimum transfer cost from launch to operational orbit. Most of the science operations will be performed while close to apogee and good communications over this long apogee period are advantageous. Nominal Proba-3 operations shall maintain a spacecraft separation of 150 m and direct the mirror towards the Sun for solar corona observations. Solar corona observations shall be restricted to apogee passage. When the two spacecraft come within 25 m, this is considered a collision.

COLLISION AVOIDANCE SCENARIOS

While collision between the two spacecraft is always possible, there are particular mission phases during which this risk becomes substantially higher as shown in Figure 2.

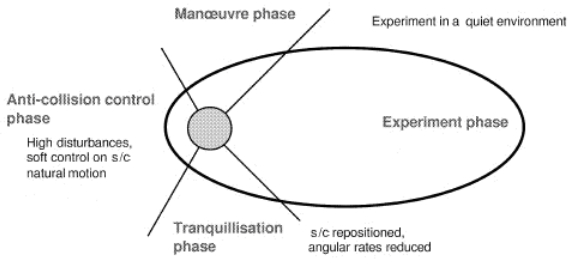

Figure 2: Mission phases along operational orbit.

These heightened risk situations are considered to occur obviously during deployment and separation, as well as during the initial commissioning phase. Deployment is considered to be the highest risk phase while during commissioning the risk arise from wrongly executed manoeuvres such as formation acquisition, formation maintenance, perigee pass and reconfiguration. During nominal operations the most demanding phase is that of formation resizing, as the spacecraft prepare to acquire the correct relative position before the start of the experiment in proximity of the apogee. Specific technology demonstrator manoeuvres such as deployment experiments or Xeus mission simulation will possibly test the collision avoidance capabilities of the formation. In general however all manoeuvres that introduce a substantial change in the inter-satellite distance can be considered to be critical. While this linear distance gives us a first feel for possible collisions it is by no means the only metric to be considered. A second, and equally important metric, to be considered is that of relative velocity. An adequate combination of relative distance and velocities will be therefore considered to be the trigger for the collision avoidance algorithms that will be assessed later.

FORMATION DYNAMICS

When describing the motion of spacecraft formations it is convenient to do so by defining the closed relative orbit geometry in terms of relative orbit element differences, rather than using the relative Cartesian coordinates of the rotating Hill coordinate frame. If the closed relative orbit is a natural solution of the relative orbital mechanics, then the corresponding orbit element difference of the deputy satellite relative to the chief satellite remains constant. Thus, the actual orbit element difference between deputy and chief satellites can be compared at any point of time to their desired values. This greatly facilitates the task of determining any relative orbit errors and correcting them. As a comparison, if a general closed relative orbit is described through some Cartesian initial conditions, then these starting values must be forward integrated to obtain the desired Cartesian coordinates of both the deputy and chief spacecraft. For some special cases it is possible to find closed form solutions to these relative orbits, such as is the case with the elliptic relative orbits obtained using the Clohessy-Wiltshire equations. However, these special solutions typically require the chief orbit to be circular and the Earth to be perfectly spherical. Using orbit element differences to describe the relative orbit does not suffer from these constraints and is thus more easily applied to the general formation flying problem. However, a relative orbit is typically sensed or measured in terms of Hill local coordinates or inertial Cartesian coordinates differences, and typically not directly in terms of orbit element differences. A direct mapping between the local Cartesian position and velocity coordinates and the osculating orbit element differences was developed in the previous chapter. This transformation is a first order approximation to the true nonlinear transformation, where it is assumed that the relative orbit dimensions are very small compared to the inertial orbits.

ORBIT VECTORS DIFFERENCE

Let us consider two spacecraft C-chief and D-Deputy, moving along similar elliptical orbits having the same semimajor axis. We want to determine the

position, velocity and acceleration of D relative to C, measured along the *xyz* frame of reference and centred on C as shown in Figure 3. From the orbital elements of the two satellites we can find the position and velocity of the two spacecraft relative to the geocentric equatorial frame of reference.

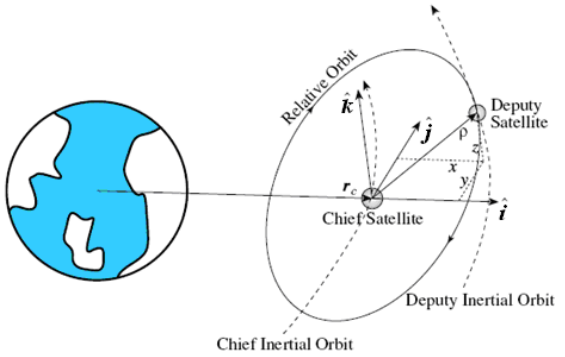

Figure 3: Hill reference geometry.

We can see that if $\mathbf{r}_d$ and $\mathbf{r}_c$ are respectively the absolute position vectors for the two spacecraft then the position of D relative to the *xyz* moving frame will be:

$$\mathbf{r}_{rel} = \mathbf{r}_d - \mathbf{r}_c \qquad [1]$$

while the velocity and acceleration will be given by:

$$\mathbf{v}_{rel} = \mathbf{v}_d - \mathbf{v}_c - \boldsymbol{\Omega} \times \mathbf{r}_{rel} \qquad [2]$$

$$\mathbf{a}_{rel} = \mathbf{a}_d - \mathbf{a}_c - \dot{\boldsymbol{\Omega}} \times \mathbf{r}_{rel} - \boldsymbol{\Omega} \times \left(\boldsymbol{\Omega} \times \mathbf{r}_{rel}\right) - 2\boldsymbol{\Omega} \times \mathbf{v}_{rel} \qquad [3]$$

where $\boldsymbol{\Omega}$ and $\dot{\boldsymbol{\Omega}}$ are the angular velocity and angular acceleration of the *xyz* frame. The relative motion between the two satellites can be transformed to the body fixed frame by means of a rotation matrix, whose components are the unit vectors of the moving frame expressed in the inertial frame

LAWDEN EQUATIONS

If the relative orbit radius is small compared with the chief orbit radius, it is possible to obtain a direct linear mapping between the Hill deputy state vector **X** and the orbit element difference vector $\delta\mathbf{e}$, such that:

$$\begin{aligned} x &= \delta r \\ y &= r\left(\delta\theta + \cos i \delta\Omega\right) \\ z &= r\left(\sin\theta - \cos\theta \sin i \delta\Omega\right) \end{aligned} \qquad [4]$$

where r is the inertial orbit radius, θ is the true latitude angle (sum of argument of perigee and true anomaly), i is the inclination angle, and Ω the right ascension of the ascending node. This set of equations represents the local Cartesian Hill frame coordinates x, y, z expressed in terms of the orbit element differences. When describing relative orbit through orbit element differences, it is not convenient however, to describe the anomaly difference through $\delta\theta$ or δf. For elliptic chief orbits, the difference in true anomaly between two orbits will vary with time even when the relative orbit is closed and bounded. To avoid this issue, the desired anomaly difference between two orbits will be expressed here in terms of a mean anomaly difference δM. This anomaly difference will remain constant, assuming unperturbed Keplerian motion with equal orbit energy states, even in the case of elliptic chief orbits. Thus Equations 4 become:

$$\begin{aligned} x(f) &= \frac{r}{a}\delta a + \frac{ae\sin f}{\eta}\delta M - a\cos f \delta e \\ y(f) &= \frac{r}{\eta^3}\left(1 + e\cos f\right)^2 \delta M + r\delta\omega + \\ &+ \frac{r\sin f}{\eta^2}\left(2 + e\cos f\right)\delta e + r\cos i\delta\Omega \\ z(f) &= r\left(\sin\theta - \cos\theta\sin i\delta\Omega\right) \end{aligned} \qquad [5]$$

where $\eta = \sqrt{1-e^2}$, ω is the argument of pericentre, e is the eccentricity, a the semimajor axis, and f is the true anomaly. Note that with this linearised mapping the difference in the argument of perigee $\delta\omega$ does not appear in the $x(f)$ expression. Further, these equations are valid for both circular and elliptic chief orbits. Only the δM and δe terms contribute periodic terms to the radial $x(f)$ solution. Due to the dependence of r on the true anomaly f, all orbit element difference terms in the along-track $y(f)$ motion contribute both static offsets as well as periodic terms. For the out-of-plane $z(f)$ motion both the δi and $\delta\Omega$ terms control the out-of-plane oscillations. These equations describe the general linearised relative motion of the deputy satellite relative to the chief in terms of orbit element differences and using true anomaly as the independent variable. The secular growth terms are hidden in the orbit element description in the orbit element differences themselves. For this common analytical case where feasible bounded relative motions are studied, the relative motion is obtained by simply sweeping the true anomaly angle from its initial state $f(t_0)$ to its final state $f(t_f)$. To relate the anomaly angle and the current time, Kepler's equation must be solved at each time step. The orbit element coordinate rates can be expressed as well in terms of orbit element differences $\{\delta a, \delta e, \delta i, \delta\Omega, \delta\omega, \delta M\}$ as:

$$\dot{x}(f) = -\frac{V_r}{2a}\delta a + \frac{V_t}{\eta^2}\sin f\left(1 + e\cos f\right)\delta e +$$

$$+ \frac{V_t}{\eta^3} e\cos f\left(1 + e\cos f\right)\delta M$$

$$\dot{y}(f) = \left[\frac{3V_t}{\eta^2}e + \frac{2h}{p}\cos f - \frac{V_r}{\eta^2}\sin f\left(2 + e\cos f\right)\right]\delta e +$$
$$+ V_r\delta\omega + V_r\cos i\,\delta\Omega - \frac{V_r}{\eta^3}\left(1 + e\cos f\right)^2\delta M - \frac{3V_t}{2a}\delta a$$
$$\dot{z}(f) = \left(V_t\cos\theta + V_r\sin\theta\right)\delta i +$$
$$+ \left(V_t\sin\theta - V_r\cos\theta\right)\sin i\,\delta\Omega \qquad [6]$$

where V_r and V_t are the chief radial and transverse velocity components, h is the chief orbit angular momentum magnitude and p is the semi-latus rectum.

Some considerations can be done on the influence each element of the difference vector has on the shape and orientation of the relative orbit. First of all, the semi-major axis difference is taken into account to avoid the spacecraft drifting apart during a complete revolution of the formation around the Earth and thus guarantee a bounded relative orbit. The semi-major axis difference is set to zero, $\delta a = 0$, for both the spacecraft, thus the periods of each satellite orbit are identical and the relative orbit is not drifting apart. Having fixed the difference in semi-major axis, the relative orbits of the formation can be found varying the remaining five Keplerian elements. The in-plane motion is governed by the difference in eccentricity, mean anomaly, argument of perigee and right ascension of the ascending node. The right ascension of the ascending node is coupling the in-plane motion with the out-of-plane motion, being $i \neq 0$. The difference in inclination is controlling only the out-of-plane motion.

MODEL COMPARISON

Having introduced two different ways with which to represent the same problem we can now perform a comparison between the two models. It is important to remember that in the vector difference model no simplification or approximation was assumed, unlike the linearisation introduced in the Lawden equations. The eccentric anomaly is at first determined using a series expansions with Bessel functions defined by:

$$E = M + \sum_{k=1}^{\infty}\frac{2}{k}J_k(ke)\sin(kM) \qquad [7]$$

where J_k are Bessel functions of the first order k:

$$J_k(ke) = \sum_{j=0}^{\infty}\frac{(-1)^j}{j!(k+j)!}\left(\frac{ke}{2}\right)^{k+2j} \qquad [8]$$

Its accuracy is determined by the order of the highest power retained in the series solution. The accuracy of the solution depends on the value of e and the order of terms considered in the expansion. Therefore, for higher values of eccentricity, the solution obtained may not be very accurate. The series expansion implemented here considers $k = 1 \ldots 10$, $j = 0 \ldots 6$. and up to e^{22}. Results are presented in Figures 4-5.

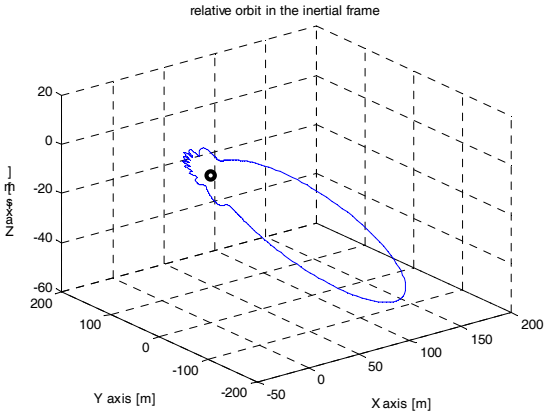

Figure 4: Relative orbit in inertial frame.

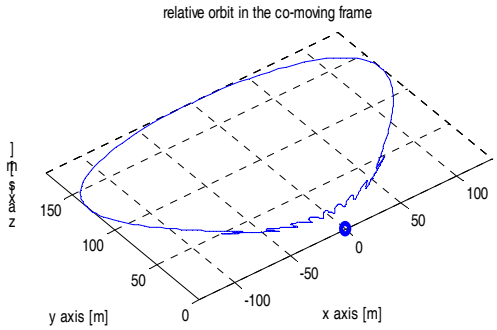

Figure 5: Relative orbit in body frame.

It is evident that, although we have considered terms up to e^{22}, this is not enough to get good results with our value of eccentricity, e = 0.830617. For this reason it is necessary to use Newton-Raphson iterative method to derive an adequate value of the eccentric anomaly through the orbital path.

Let us first consider the case of modifying all the three parameters influencing the orbit's orientation ($\delta\omega$, $\delta\Omega$, δi) through the vector difference model. Results are shown in Figures 6-9.

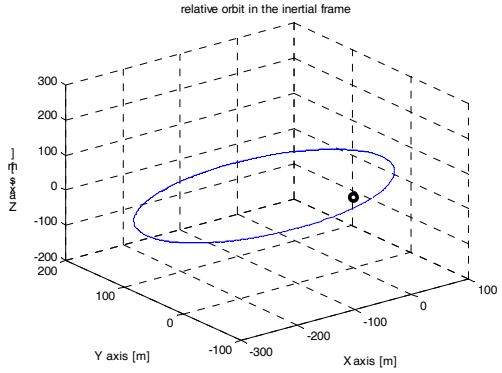

Figure 6: Relative orbit in inertial frame.

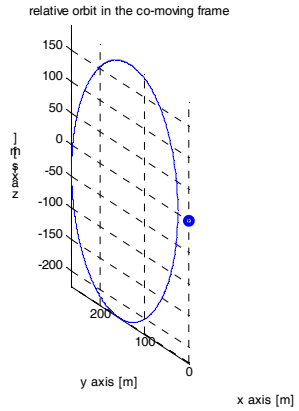

Figure 7: Relative orbit in body frame.

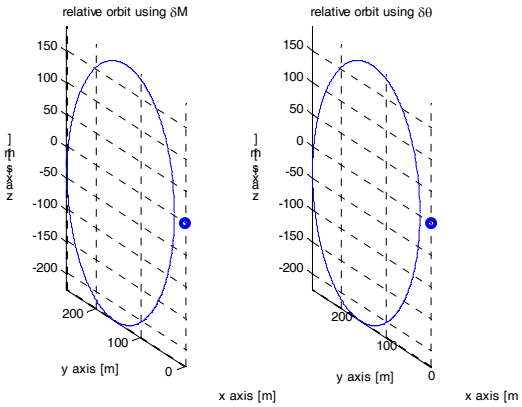

Figure 10: Relative orbit in body frame.

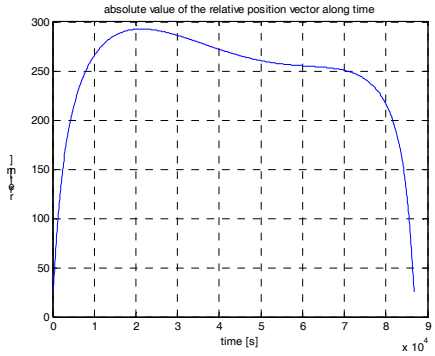

Figure 8: Relative position vector.

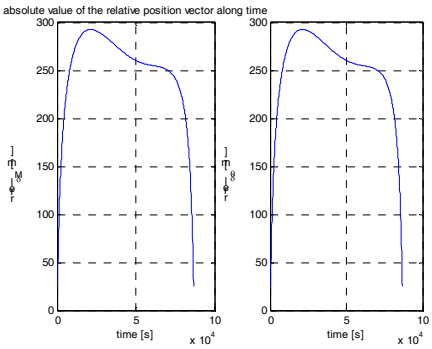

Figure 11: Relative position vector.

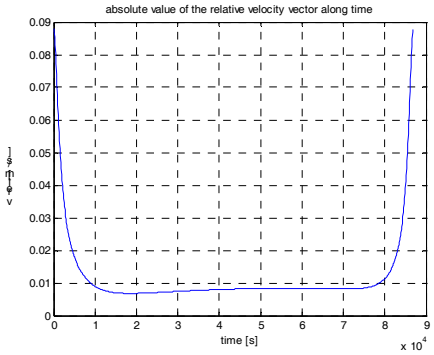

Figure 9: Relative velocity vector.

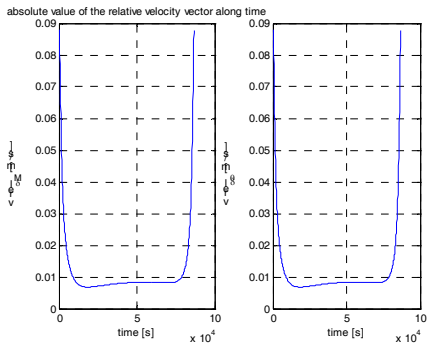

Figure 12: Relative velocity vector.

In order to get the relative orbit between the two spacecraft Lawden equations are solved through orbit element differences shown in Equations 4 and 5. There are two sets of orbit element differences we can use: (δa, δe, $\delta\omega$, δi, $\delta\Omega$, δM) and (δa, δq_1, δq_2, δi, $\delta\Omega$, $\delta\theta$). The two linearized analytical systems of equations expressed in terms of the two sets of orbit element differences represent the solutions of the Lawden equations. For unperturbed Keplerian orbits, the anomaly difference in mean anomaly δM is constant, like the other orbital element differences, while the anomaly difference in true latitude $\delta\theta$ (with $\theta = f + \omega$) varies throughout the orbit, as we consider elliptic orbits. Let us again consider the case of modifying all the three parameters influencing the orbit's orientation ($\delta\omega$, $\delta\Omega$, δi). Results are shown in Figures 10-12.

From the comparison between the two models, using the same values for the orbit element differences, we get the same results. This is a confirmation that, the use of the first order linearised expression of the equation of motion, employed for Lawden equations, is widely justified.

FORMATION CONTROL

In order to maintain a satellite formation, a control system must be designed to compensate for the deviation of the motion of the satellites from the desired trajectories. Control algorithms are also necessary, for establishing and reconfiguring formations. Continuous time control is more suitable for tracking the desired relative orbits that may or may not be natural solutions to the relative motion dynamics. Continuous time control seeks to establish

zero tracking errors at all times. On the other hand impulsive control can manages errors within an appropriate threshold. Traditionally, impulsive control has been found to be more suitable for orbit corrections, and is done on a periodic basis. the complete nonlinear equations of relative motion dynamics between a chief satellite in an elliptical orbit and a deputy, can be written as follows

$$\ddot{x} - 2\dot{f}\left(\dot{y} - y\frac{\dot{r}_c}{r_c}\right) - x\dot{f}^2 - \frac{\mu}{r_c^2} = -\frac{\mu}{r_d^3}\left(r_c + x\right) + u_x$$

$$\ddot{y} + 2\dot{f}\left(\dot{x} - x\frac{\dot{r}_c}{r_c}\right) - y\dot{f}^2 = -\frac{\mu}{r_d^3}y + u_y \qquad [9]$$

$$\ddot{z} = -\frac{\mu}{r_d^3}z + u_z$$

where n is the mean motion of the chief, and u_x, u_y, u_z are the external controls. The system of equations presented above involves ten states and the full-fledged effects of both nonlinearity and eccentricity are accounted for. The effects of eccentricity of the reference orbit that influences the relative motion dynamics of the deputy are captured by the augmented fourth order dynamics of the chief. This model is referred to as the 'true model', as the equations are presented in their exact nonlinear form, with no approximation or simplification. A controller is required to stabilize the relative motion dynamics. In the following section, continuous controllers are introduced.

PERIOD MATCHING CONTROL

The relative motion between two Earth orbiting spacecraft will always be bounded if the period of the two spacecraft is the same. Period-matching is equivalent to matching the energy of the two spacecraft. Energy-matching results in bounded relative orbits that are natural and hence consume zero fuel in steady state. The relative motion initial conditions determine the energy of the deputy, given the initial conditions of the chief. There exist energy matched manifolds in the state-space of relative motion dynamics, that result in bounded relative orbits. However the HCW initial conditions in general do not lie on these manifolds. This constitutes the reason for the breakdown of the HCW solutions. The period matched initial conditions and the manifolds cannot be analytically solved for. However, the criterion for period matching can be written as a constraint in terms of the relative motion coordinates. By stabilizing this constraint, we can draw the trajectory originating from HCW initial conditions to the nearest period matched trajectory. We now develop the constraint and the stabilizing control law. Considering the differential energy between chief and deputy orbital energy $\delta E = E_d - E_c$ the energy matching requirements can be attained by imposing the following constraints of the relative motion dynamics:

$$\delta\dot{E} + k\delta E = 0 \qquad [10]$$

Since the chief is in a two-body orbit, its energy is constant. Hence, the derivative of the difference in the energies of the two spacecraft can be written as:

$$\delta\dot{E} = \dot{E}_d \qquad [11]$$

In the absence of external disturbances a control strategy that ensures $\dot{E}_d = 0$ is required. Since we have three possible controls: u_x, u_y and u_z, but only one constraint we can arbitrarily chose two to be equal to zero. We can therefore obtain the control u_y to stabilise Eq 10 as:

$$u_y = k\frac{\left[\frac{v_c^2 - v_d^2}{2} + \mu\left(\frac{1}{r_d} - \frac{1}{r_c}\right)\right]}{\dot{y} + \omega x + V_t} \qquad [12]$$

The period-matching controller will only result in relative orbits that are natural solutions to the family of zero differential energy solutions.

POTENTIAL FUNCTION CONTROL

The potential function method is an extension of Lyapunov's second method and has found several applications in the field of space systems engineering. Given a set of differential equations $\dot{\mathbf{y}} = \mathbf{f}(\mathbf{x})$, which describe the time evolution of a dynamic system, and defining the desired final state, the convergence to this state and the global stability of the system can be guaranteed by building a Lyapunov potential function that has a global minimum in the final state. The aim is to bring the spacecraft to the desired location, avoiding any risks of collision. The terms that must be controlled therefore are the position and velocity vectors of the chaser. The potential function used here consists of two attractive terms. The first one controls the position while the second one controls the velocity:

$$\mathbf{V} = \mathbf{V}_\mathrm{p} + \mathbf{V}_\mathrm{v} \qquad [13]$$

where

$$\mathbf{V}_p = \frac{1}{2}\sum_{1=1}^{3}\alpha_i\left(\mathbf{r}_i - \mathbf{r}_{goal}\right)^2 \qquad [14]$$

$$\mathbf{V}_v = \frac{1}{2}m\sum_{1=1}^{3}\alpha_i\left(\mathbf{v}_i - \mathbf{v}_{goal}\right)^2 \qquad [15]$$

where m is the spacecraft mass, $\mathbf{r}_i$ and $\mathbf{v}_i$ the current position and velocity vectors of the spacecraft, $\mathbf{r}_{goal}$ and $\mathbf{v}_{goal}$ the desired position and velocity vectors and α is a shaping parameter. Note that there is no repulsive term in the potential function. The mission consists only of two spacecraft, which must maintain an average distance, when operational during the science phase of 150 m. Imposing this formation-keeping between the two satellites, automatically implies the satisfaction of the collision avoidance requirement.

REAL-TIME POSITION CONTROL

This control methodology originates in the field of manipulator robotics. A safety zone is defined around the robot and virtual forces represent the intrusion of the manipulator into the obstacle zone. This method hinges on the definition of a velocity vector $\mathbf{v}$ to allow the reaching of the desired goal position ensuring collision avoidance

$$\mathbf{v} = \mathbf{v}_d + \mathbf{v}_{obs} \qquad [16]$$

where $\mathbf{v}_d$ is the desired velocity vector and $\mathbf{v}_{obs}$ is a PID controller defined as:

$$\mathbf{v} = k\left(k_P\mathbf{d} + k_I \int \mathbf{d} + k_D \frac{d\mathbf{d}}{dt} \right) \qquad [17]$$

where the vector $\mathbf{d}$ defines the obstacle zone as the difference between the current spacecraft position and a chosen detection sphere:

$$\mathbf{d} = \mathbf{r}_{obs} - \mathbf{r}_{sc} \qquad [18]$$

GYROSCOPIC CONTROL

This approach uses gyroscopic forces to drive the spacecraft away from an obstacle without modifying the nominal path. The method hinges on defining a velocity vector $\mathbf{v}$, comprising three components: a desired velocity, a dissipative velocity and a gyroscopic velocity:

$$\mathbf{v} = \mathbf{v}_d + \mathbf{v}_{diss} + \mathbf{v}_{gyro} \qquad [19]$$

where the dissipative and gyroscopic components are PID controllers:

$$\mathbf{v}_{diss} = k_{PD}\mathbf{v}_{d^*} + k_{ID}\int \mathbf{v}_{d^*} + k_{DD}\frac{d\mathbf{v}_{d^*}}{dt} \qquad [20]$$

$$\mathbf{v}_{gyro} = k_{PG}\mathbf{v}_{g^*} + k_{IG}\int \mathbf{v}_{g^*} + k_{DG}\frac{d\mathbf{v}_{g^*}}{dt} \qquad [21]$$

where

$$\mathbf{v}_{d^*} = K\mathbf{v}_{sc}\left(e^{-\mathbf{r}_{sc}} - e^{-\mathbf{r}_{obs}}\right) \qquad [22]$$

$$\mathbf{v}_{g^*} = M\mathbf{v}_{sc} \qquad [23]$$

with K and M being shaping parameters.

NUMERICAL RESULTS

We will now evaluate the different control strategies introduced earlier to assess their suitability in meeting the mission requirements. That is, ensure an operational distance between the spacecraft of at least 150m while avoiding any collision. Results are presented in Figures 13-15 for the period matching approach, Figures 16-19 for the potential function control, Figures 20-22 for the real-time positioning control and Figures 23-25 for the gyroscopic control.

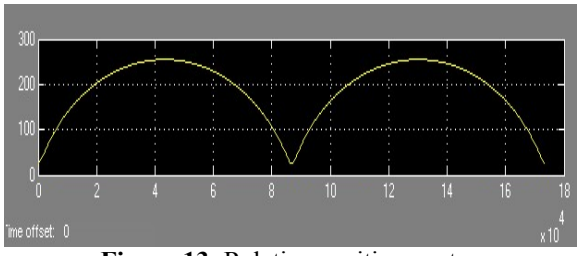

Figure 13: Relative position vector.

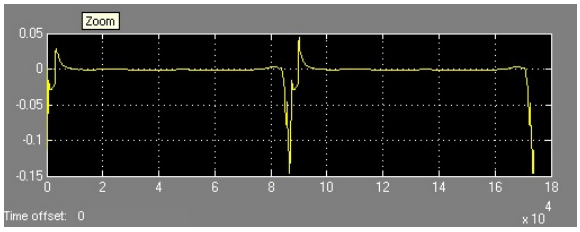

Figure 14: Differential energy.

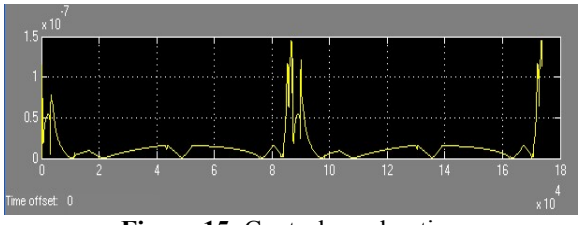

Figure 15: Control acceleration

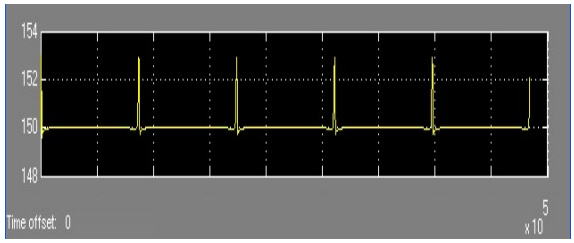

Figure 16: Relative position vector.

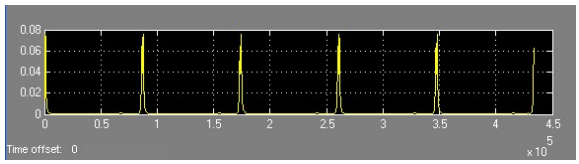

Figure 17: Potential.

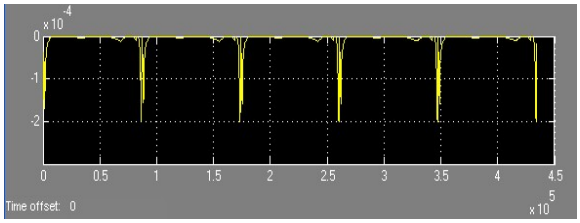

Figure 18: Potential derivate.

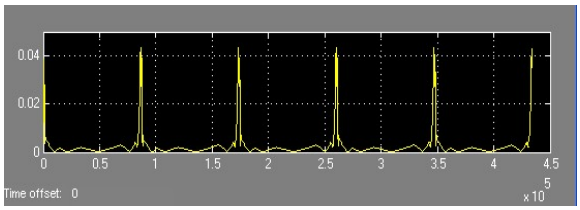

Figure 19: Control force.

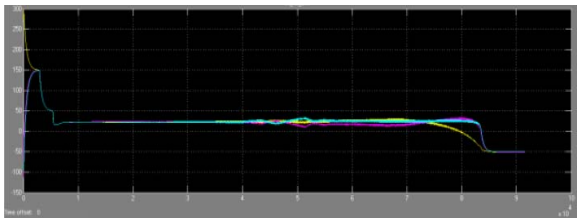

Figure 20: Relative position vector.

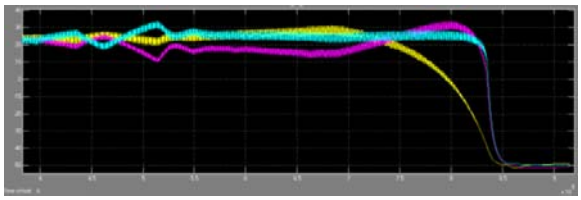

Figure 21: Close up of relative position vector.

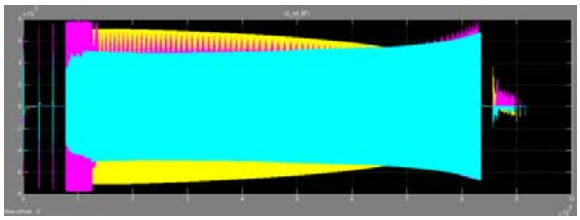

Figure 22: Control accelerations.

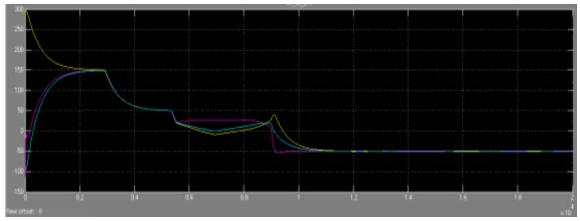

Figure 23: Relative position vector.

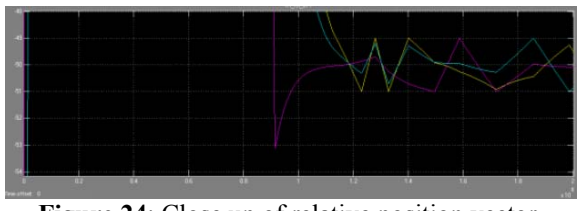

Figure 24: Close up of relative position vector.

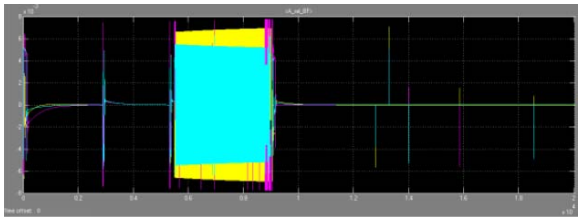

Figure 25: Control accelerations.

It can be sent that all controllers are capable of meeting the mission requirements. A number of considerations can however be made. The real-time positioning control, while successful, requires a substantial amount of time to reach convergence; close to one orbit and this is clearly not acceptable. In addition to this, this method produces substantial oscillations in the velocity and acceleration vectors, indicative of an intense actuator activity. The potential function and gyroscopic control both appear more promising as they both converge in comparable times. The potential function control however appears to be less demanding on the actuators. Finally the period-matching control law does not represent appear to be a valid alternative. The reason being that we obtain natural relative orbits and hence consume zero fuel. However since the relative orbit obtained is a natural orbit, the trend of the relative position vector along time is sinusoidal, and not constant, as would be desired. Practically this controller transfers the Hill-Clohessy-Wiltshire initial conditions to the nearest period matched initial conditions. Therefore using this approach with the HCW initial conditions is equal to having no control law but using the initial conditions including the bounded condition for the eccentricity.

CONCLUSIONS

This work presented here implemented different algorithms for the spacecraft formation reconfiguration and collision avoidance, taking Proba-3 as a test case. The contributions of this thesis are as follows. We introduced linearised and nonlinear models for the relative motion dynamics of a formation flying. One based on the relative motion kinematic equations the other using orbit element differences. Both models produce the same results with regards to the dynamics of the system. Different continuous control methods, that maintain and stabilize the formation, have been introduced. These methods provide the basis for a computationally efficient autonomous guidance and control system. The results show the benefits and drawbacks of the different control strategies. Potential function and gyroscopic control appear to be the most promising options. Further work will focus on introducing gravitational and solar radiation pressure disturbances as well as addressing the issue of fuel consumption.